

Chinese Journal of Chemical Engineering

Pyrolyzing soft template-containing poly(ionic liquid) into hierarchical N-doped porous carbon for electroreduction of carbon dioxide

--Manuscript Draft--

Manuscript Number:	CJCHE-D-21-00390
Article Type:	Research Paper
Section/Category:	Catalysis, kinetics and reaction engineering
Keywords:	CO ₂ RR; poly(ionic liquid); N-doped carbon materials; pore diameter; hierarchical pore
Corresponding Author:	Jun Wang Nanjing Tech University Nanjing, China
First Author:	Mingdong Sun
Order of Authors:	Mingdong Sun Zhengyun Bian Weiwei Cui Xiaolong Zhao Shu Dong Xuebin Ke Yu Zhou Jun Wang
Abstract:	<p>Heteroatom doped carbon materials have demonstrated great potential in the electrochemical reduction reaction of CO₂ (CO₂ RR) due to the versatile structure and function. However, rational structure control still remains one challenge. In this work, we reported a unique carbon precursor of soft template-containing porous poly(ionic liquid) (PIL) that was directly synthesized via free-radical self-polymerization of ionic liquid monomer in a soft template route. Variation of the carbonization temperature in a direct pyrolysis process without any additive yielded a series of carbon materials with facile adjustable textural properties and N species. Significantly, the integration of soft-template in the PIL precursor led to the formation of hierarchical porous carbon material with a higher surface area and larger pore size than that from the template-free precursor. In CO₂ RR to CO, the champion catalyst gave a Faraday efficiency of 83.0% and current density of 1.79 mA cm⁻² at -0.9 V vs. reversible hydrogen electrode (vs. RHE). The abundant graphite N species and hierarchical pore structure, especial the unique hierarchical small-/ultra-micropores were revealed to enable the better CO₂ RR performance.</p>
Suggested Reviewers:	<p>Yufei Song Beijing University of Chemical Technology songyf@mail.buct.edu.cn He is engaged in research on catalyst design</p> <p>Youting Wu Nanjing University ytwu@nju.edu.cn He is engaged in research on carbon dioxide conversion</p> <p>Zhengbao Wang Zhejiang University zbwang@zju.edu.cn He is engaged in research on catalyst design</p> <p>Yanqin Wang East China University of Science and Technology</p>

	wangyanqin@ecust.edu.cn She is engaged in research on catalyst design
	Jianguo Wang Zhejiang University of Technology jgw@zjut.edu.cn He is engaged in research on catalyst design
	Qin Zhong Nanjing University of Science and Technology zq304@mail.njust.edu.cn He is engaged in research on catalyst.

Statement for the submission to *Chinese Journal of Chemical Engineering*

Dear editor,

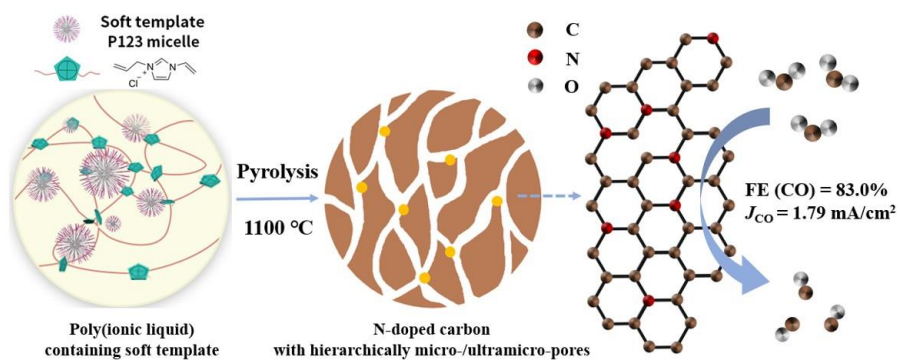
I am submitting the manuscript to Chinese Journal of Chemical Engineering for your consideration for its possible publication. It is authored by Mingdong Sun, Zhengyun Bian, Weiwei Cui, Xiaolong Zhao, Shu Dong, Xuebin Ke, Yu Zhou, and Jun Wang, with the title of "Pyrolyzing soft template-containing poly(ionic liquid) into hierarchical N-doped porous carbon for electroreduction of carbon dioxide". We guarantee that the manuscript is our original work and each author agrees this submission, and it has not been published in any other media.

Electrochemical reduction reaction of carbon dioxide (CO₂RR) has become greatly significant for the control of the carbon cycle in the earth and sustainable production of chemicals and fuels. Various metal-free carbon materials have been developed for CO₂RR to CO due to the advantages such as earth-abundant element, low cost, non-toxicity, adjustable pore structure, and chemical composition. However, it still remains one challenge to rationally design efficient carbon materials for CO₂RR. Porous poly(ionic liquid) (PIL) is a family of organic polymers that combines the advantages of porous organic polymers (POPs) and ionic liquid (IL). Because of the high thermal stability, molecular designability, and abundant heteroatoms in the matrix, various PILs have been applied as precursors to produce heteroatom-doped carbon materials without extra heteroatom resources. PIL-derived carbon materials have been applied in the adsorption, separation, and catalysis fields, but their behavior in CO₂RR is still to be explored, so far. Herein, we report the first example of the soft template-containing PIL-derived N-doped carbon, and its catalysis behavior in CO₂RR to CO. The result demonstrates the vital role of PIL precursor's internal property in the structure and function modulation of the resultant carbon, which is crucial to its better performance in CO₂RR.

In this work, the PIL precursor was synthesized *via* the free radical self-polymerization of IL monomer 1-allyl-3-vinylimidazole chloride by using triblock copolymer P123 as the soft-template. Direct carbonization of the template-containing PIL precursor at different pyrolysis temperatures yielded a series of N-doped carbon materials with controllable porous structure and N species. It was found that the template-containing precursor led to a unique hierarchically micro-/ultra-microporous structure, whereas the template-free counterpart produced microporous carbon with smaller surface area and pore size. The champion carbon exhibited a CO₂RR-to-CO faraday efficiency of 83% and a current density of 1.79 mA cm⁻² at -0.9 V *vs.* reversible hydrogen electrode (*vs.* RHE). The formation of abundant graphitic N species and hierarchical micro-/ultra-micropores are revealed to be responsible for such a considerably high CO₂RR activity by facilitating the mass transfer, providing large electrochemical active sites, and promoting the contact between reactants and active sites through remarkable nano-confinement effect. This work demonstrates a new avenue to fabricate metal-free carbon for CO₂RR and highlights the potential of the single component PIL as a versatile carbon resources to regulate the pore structure and catalytic behavior of carbon-based electrocatalysts.

Thank you for your kind considerations.

Sincerely yours,
Prof. Dr. Jun Wang



Highlights

1. Soft template-containing poly(ionic liquid) was pyrolyzed to N-doped carbon.
2. Porosity and N species were modulated by controlling pyrolysis temperatures.
3. The resultant carbon featured hierarchically small-/ultra-microporous structure.
4. The champion carbon exhibited considerably high activity for CO₂RR to CO.
5. Hierarchical small-/ultra-micropores accounted for the electrocatalysis activity.

Pyrolyzing soft template-containing poly(ionic liquid) into hierarchical N-doped porous carbon for electroreduction of carbon dioxide

Mingdong Sun^{1†}, Zhengyun Bian^{1†}, Weiwei Cui^{1†}, Xiaolong Zhao¹, Shu Dong¹, Xuebin Ke², Yu Zhou^{1*}, Jun Wang^{1*}

¹State Key Laboratory of Materials-Oriented Chemical Engineering, College of Chemical Engineering, Nanjing Tech University, Nanjing, 210009, China

²Department of Chemical Engineering, University of Hull, Hull, HU6 7RX, United Kingdom

***Corresponding Authors**

E-mail: njtzhouyu@njtech.edu.cn (Y. Zhou); junwang@njtech.edu.cn (J. Wang).

[†]These three authors contributed equally: M. Sun, Z. Bian, and W. Cui.

Pyrolyzing soft template-containing poly(ionic liquid) into hierarchical N-doped porous carbon for electroreduction of carbon dioxide

Mingdong Sun^{1†}, Zhengyun Bian^{1†}, Weiwei Cui^{1†}, Xiaolong Zhao¹, Shu Dong¹, Xuebin Ke², Yu Zhou^{1*}, Jun Wang^{1*}

¹State Key Laboratory of Materials-Oriented Chemical Engineering, College of Chemical Engineering, Nanjing Tech University, Nanjing, 210009, China

²Department of Chemical Engineering, University of Hull, Hull, HU6 7RX, United Kingdom

*Corresponding Authors

E-mail: njtzhouyu@njtech.edu.cn (Y. Zhou); junwang@njtech.edu.cn (J. Wang).

[†]These three authors contributed equally: M. Sun, Z. Bian, and W. Cui.

Abstract:

Heteroatom doped carbon materials have demonstrated great potential in the electrochemical reduction reaction of CO₂ (CO₂RR) due to the versatile structure and function. However, rational structure control still remains one challenge. In this work, we reported a unique carbon precursor of soft template-containing porous poly(ionic liquid) (PIL) that was directly synthesized *via* free-radical self-polymerization of ionic liquid monomer in a soft template route. Variation of the carbonization temperature in a direct pyrolysis process without any additive yielded a series of carbon materials with facile adjustable textural properties and N species. Significantly, the integration of soft-template in the PIL precursor led to the formation of hierarchical porous carbon material with a higher surface area and larger pore size than that from the template-free precursor. In CO₂RR to CO, the champion catalyst gave a Faraday efficiency of 83.0% and current density of 1.79 mA cm⁻² at -0.9 V *vs.* reversible hydrogen electrode (*vs.* RHE). The abundant graphite N species and hierarchical pore structure, especial the unique hierarchical small-/ultra-micropores were revealed to enable the better CO₂RR performance.

Keywords: CO₂RR, poly(ionic liquid), N-doped carbon materials, pore diameter, hierarchical pore

1. Introduction

As one of the main greenhouse gases with continuous growing concentration in the atmosphere, carbon dioxide (CO₂) is indeed a cheap and renewable C1 resource [1, 2]. Catalytic conversion of CO₂ into valuable chemicals and fuels is of great significance to alleviate the energy and environmental crisis [3, 4]. Among various strategies, electrochemical reduction reaction of CO₂ (CO₂RR) is greatly attractive because of the favorable operation under mild conditions and the advantages in energy storage by using renewable clean energy such as solar and wind [5-7]. However, the development of highly effective electrocatalysts remains one challenge due to the sluggish of inert CO₂ molecules and the inevitable competing hydrogen evolution reaction (HER) in aqueous media.

Various metal-based electrocatalysts, especially noble metals, like Au, Pd and Ag, have been established for CO₂RR process [8-11], which still suffered from high cost, limited resource, or environmental unfriend [12, 13]. This situation motivates the development of metal-free electrocatalysts such as non-metallic inorganics [14], biomass [15], polymers [16], carbon materials [13, 17-19], etc. Especially, N-doped porous carbon (NPC) was extensively studied because of the abundant natural resource, large surface area, good conductivity, high stability, and tunable functionality [12, 20]. Their electro-catalytic performance for CO₂RR associates closely with type, density, dispersion of N species, plus porosity and morphology. Modulation of these structural characters strongly depends on the precursors and the preparation method. For example, N resources were normally externally added to integrate N species into porous carbon *via* pyrolysis [21]. On the other hand, hard/soft template or metal salts activation was used to create abundant hierarchical porosity in NPC for improving mass transfer [22].

Despite much progress, it is still challenging to rationally design carbon electrocatalysts with controllable N species and porosity. We note that the facile preparation of NPC *via* direct pyrolysis of N-containing precursors favors improving the dispersion and stability of N species and fabricating hierarchical porous structure [23]. Nonetheless, the qualified carbon precursors to render this issue are rare, so far.

Ionic liquids (ILs), especially the most popular imidazolium based ILs, have been employed as the NPC precursors for decades, due to their negligible vapor pressure, high thermal stability, and inherently N-doping structures [24-26]. In principle, porous precursors exemplified by porous organic polymers (POPs) are attractive to controllably obtain porous carbon *via* pyrolysis [27]. Actually, porous poly(ionic liquid) (PIL), combining the advantages of ILs and POPs, are emerging as a novel family of carbon precursors with task-specific design of cations and anions, facile doping of N species, and possible tuning of pore structures [28]. As afore we noticed, N species and porous structure are two key factors for NPC-based CO₂RR process, it is thus rational to say that PIL-derived carbon materials are highly desirable for this reaction. Indeed, PIL-derived carbon materials have been applied in CO₂ adsorption [29], energy storage [30], and catalysis [31, 32]. For instance, the N, P dual-doped carbon prepared by pyrolyzing poly[vinyl imidazolium dihydrogen phosphate] was reported as an active metal-free electrocatalyst for oxygen reduction reaction (ORR) [32]. For CO₂RR to formate, a nanoporous polymer/CNTs membrane was fabricated by coating poly[1-cyanomethyl-3-vinylimidazolium bis(trifluoromethanesulfonyl)imide] on carbon nanotubes followed with an ammonia treatment, the carbonization of which gave a hierarchical porous nitrogen-doped carbon/CNTs composite showing a Faradaic efficiency (FE) of 81% [31]. To the best of our knowledge, the application of PIL-derived carbon materials in CO₂RR is much limited and to be explored.

In this work, we task-specifically prepared the hierarchically porous NPC material by pyrolyzing the PIL precursor and proved its efficiency for CO₂RR process. The PIL precursor was synthesized from the free radical self-polymerization of the ILs monomer 1-allyl-3-vinylimidazolium chloride in the presence of block copolymer P123 as the soft template, according to our previous work [33]. Rather than the pre-removal of the soft template by a solvent, the P123-containing PIL was directly subjected to pyrolysis for obtaining the target NPC. Systematic characterizations suggest that considerable amounts of N species remained at the high pyrolysis temperature beyond 1000 °C and the formation of hierarchical pore structure arose from the soft template. For CO₂RR, the resultant NPC material exhibited a high FE towards CO (83.0%), and the property-activity relationship was analyzed and discussed in details.

2. Experimental

2.1 Materials and methods

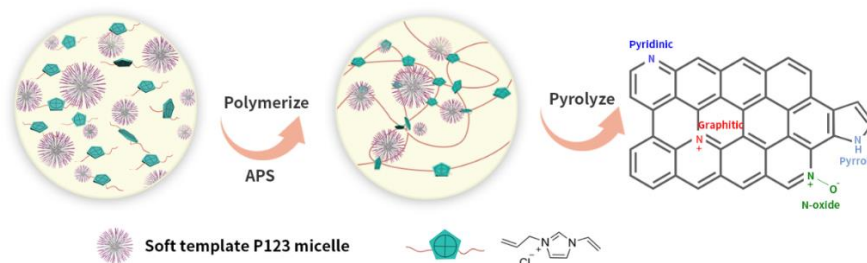
ILs monomer, 1-allyl-3-vinylimidazolium chloride ([AVIM]Cl, ≥99%), was purchased from Lanzhou Greenchem ILs, LICP, Chinese Academy of Sciences. Triblock copolymer poly(ethylene glycol)-block-poly (propylene glycol)-block-poly (ethylene glycol) (P123, M_w=5800) was purchased from Sigma-Aldrich. Polyethylene glycol (PEG, M_w=20000) was bought from Xilong Science Co. Ltd. Ammonium persulfate (APS, >98%) was purchased from Shanghai Lingfeng Chemical Reagent Co. Ltd. Potassium bicarbonate (KHCO₃, 99.99%) was obtained from Shanghai Macklin Biochemical Co. Ltd. Nafion solution (5.0 wt.%) was available from DuPont. All chemical substances were used as received without further purification.

X-ray photoelectron spectroscopy (XPS) was performed on a PHI 5000 Versa Probe X-ray photoelectron spectrometer equipped with Al K α radiation (1486.6 eV). Thermogravimetric (TG) analysis was carried out on an STA409 instrument under the

nitrogen atmosphere at a heating rate of $10\text{ }^{\circ}\text{C min}^{-1}$. X-ray diffraction (XRD) patterns were collected on a Smart Lab diffractometer (Rigaku Corporation) equipped with a 9 kW Cu rotating-anode source. Nitrogen sorption isotherms and pore size distribution curves were measured at -196°C on a BELSORP-MINI analyzer. Scanning electron microscopy (SEM) images were acquired with a Hitachi S-4800 scanning electron microscope (10 kV). Transmission electron microscopy (TEM) images were collected on a JEOL JEM-2100 apparatus (200 kV). Fourier transform infrared spectra (FTIR) were recorded on an Agilent Cary 660 instrument. Elemental compositions were analyzed on a Vario EL cube CHN elemental analyzer. Raman spectra were recorded on a Horiba HR 800 spectrometer with a Spectra-Physics 2018 Argon/Krypton Ion Laser system (excitation line: 514 nm). Quantitative analysis of liquid products after electrolysis of the electrolyte was carried out by nuclear magnetic resonance.

2.2 Materials synthesis

2.2.1 Preparation of PIL precursor



Scheme 1. Synthetic route of porous poly(ionic liquid) CAV and the corresponding derived carbon materials.

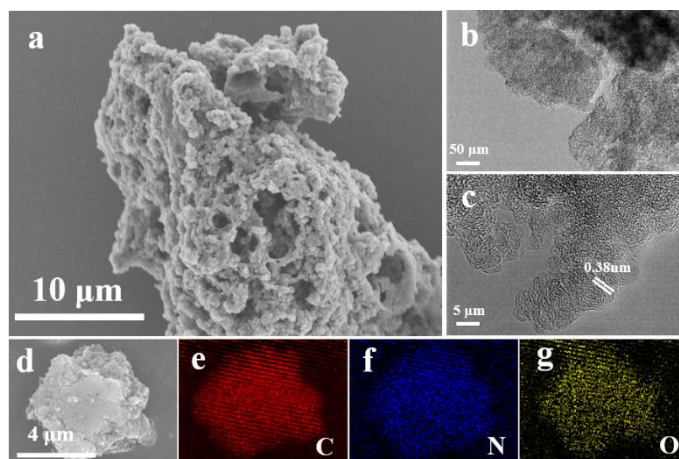


Fig. 1 (a) SEM image, (b, c) TEM images, and (d-g) SEM elemental (C, N, and O) imagings of PAC-1100.

Self-polymerization of [AVIM]Cl was carried out in a modified soft-template pathway following a previous report [33]. In a typical synthesis, P123 (2 g), PEG (1 g), and H₂O (8 g) were added into a 50 mL beaker and stirred at room temperature for 24 h, followed by the addition of [AVIM]Cl (2 g) and additional stirring for 24 h. The polymerization occurred at 40 °C for 10 h and then 50 °C for 14 h after the addition of APS (7 g) as initiator. The formed white solid was isolated by filtration and washed with deionized water, and then vacuum dried at 60 °C to give the PIL precursor, named CAV. For comparison, nonporous counterpart CAV-N was synthesized in the absence of P123 and PEG.

2.2.2 Preparation of PIL-derived carbon materials

PIL-derived carbon materials were prepared by a one-step pyrolysis method by using CAV as the carbon resource. Specifically, CAV (2 g) was placed into a crucible at the center of the atmosphere furnace, the temperature of which was raised to the desired pyrolysis temperatures at a rate of 2 °C min⁻¹ under N₂ atmosphere with a flow rate of 200 mL min⁻¹ and maintained for 2 h. The obtained carbon materials were denoted as PAC-T, where T represents the pyrolysis temperature. Thus, carbon materials prepared via pyrolysis of CAV at six different temperatures of 800 °C, 900 °C, 1000 °C, 1100 °C,

1200 °C were denoted as PAC-800, PAC-900, PAC-1000, PAC-1100, PAC-1200, respectively. And pyrolysis of CAV-N at 1100 °C gave the carbon materials of ntPAC-1100.

2.3 Electrochemical measurements

2.3.1 Preparation of working electrode

Typically, well ground catalyst powder (5 mg) was dispersed in a mixture of Nafion solution (5 wt.%, 40 μL) and ethanol (400 μL) *via* ultrasonication for 30 min. Subsequently, the obtained catalyst ink (88 μL) was dropped onto the carbon paper substrate electrode (coating area: 1×1 cm), and then dried at 30 °C to give the working electrode with a catalyst mass loading of 1 mg cm^{-2} .

2.3.2 Electrochemical reduction of CO₂

All the electrochemical experiments were carried out on a CHI 760E electrochemical workstation (Shanghai Chen-Hua, China) by using a gas-tight two-compartment H-cell equipped with a standard three-electrode configuration. The three-electrode systems included a working electrode as prepared above, an Ag/AgCl electrode (filled with 3.5 mol L^{-1} KCl) as the reference electrode, and a Pt plate (1×1 cm) as the counter electrode. The former two electrodes were placed in the cathode chamber, while the latter one was placed in the anode chamber. Each compartment was filled with ~ 50 mL electrolyte (0.1 mol L^{-1} KHCO₃ aqueous solution) and separated by a piece of Nafion 117 proton exchange membrane to avoid the re-oxidation of CO₂RR-generated products. The measured potentials were rescaled to the reversible hydrogen electrode (RHE) according to the following equation: $E (\text{vs. RHE}) = E (\text{vs. Ag/AgCl}) + 0.2046 \text{ V} + 0.059 \text{ V} \times \text{pH}$. All the mentioned potentials were referred to the RHE unless otherwise noted.

Before the electrolysis experiment, the cathodic chamber was bubbled with high-

purity CO₂ (99.9999%, 40 mL min⁻¹) for 30 min to remove O₂ from the electrolyte and saturate the electrolyte with CO₂. Electrochemical reduction of CO₂ was carried out at each applied potential for 30 min under ambient conditions. The current density (*j*) was normalized to the geometrical area of the working electrode (1 cm²). The gas-phase was analyzed by a gas chromatograph (GC-9860-5CNJ, Nanjing Hope Analytical Equipment Co., LTD, China) equipped with a flame ionization detector (FID), a thermal conductivity detector (TCD), and a 5A molecular sieve packed column (2 m). Only CO and H₂ were detected in this study. After the potentiostat electrolysis, 800 μL catholyte was mixed with 100 μL D₂O and then analyzed by ¹H nuclear magnetic resonance (¹H NMR) spectrometer (Bruker DPX 500 MHz), showing that no liquid product formed. Faraday efficiency (FE) of gaseous products at each applied potential was calculated based on the equation: FE (%) = (*z* × *n* × F) / Q × 100%, where *z* is the number of the transferred electron to produce a molecule of the gas product; *n* is the moles of the formed gas product; F is the Faraday constant (96485 C mol⁻¹); Q is the total charge acquired from the electrochemical workstation.

Linear sweep voltammetry (LSV) measurements were performed in N₂- or CO₂-saturated 0.1 mol L⁻¹ KHCO₃ electrolyte with a scan rate of 5 mV s⁻¹. The pH of the CO₂-saturated 0.1 mol L⁻¹ KHCO₃ electrolyte was 6.8. Cyclic voltammetry (CV) was performed at the potential range 0 to 0.5 V in an N₂-saturated 0.1 mol L⁻¹ KHCO₃ solution with different scan rates, giving the double-layer capacitance (*C*_{dl}) for the determining of electrochemical surface area (ECSA). *C*_{dl} value is calculated by plotting Δ*J* (*J*_a-*J*_c) as a function of scan rate, in which *J*_a and *J*_c are anode and cathode current densities, respectively. The slope of the line is twice that of *C*_{dl}. Electrochemical impedance spectroscopy (EIS) was tested at the -0.9 V in the frequency range from 0.01 Hz to 100 kHz with a voltage amplitude of 10 mV.

3. Results and discussion

3.1 Synthesis and characterization of carbon materials

Scheme 1 illustrates the preparation procedure for the PIL CAV and the resultant carbon materials. The precursor CAV was synthesized via the free radical self-polymerization of ionic liquid monomer 1-allyl-3-vinylimidazolium chloride ([AVIM]Cl) by using ammonium persulfate (APS) as the initiator and P123 as the soft template. The Fourier transform infrared (FT-IR) spectrum of CAV (Fig. S1) showed characteristic bands of the imidazole group with the disappearance of the C=C bond, evidencing the polymerization of [AVIM]Cl. The thermogravimetric (TG) curve of CAV (Fig. S2) presented a shape weight loss from 200 °C to 500 °C due to the removal of the template with the possible partial decomposition of the polymeric skeleton. The weak weight loss above 500 °C reflects the high thermal stability. Without pre-removing of the soft-template, direct pyrolysis of CAV at different temperatures (T=800, 900, 1000, 1100, and 1200) yielded a series of N-doped carbon materials, termed PAC-T. Various characterization techniques were applied to reveal the structural information of PAC-T. Scanning electron microscopy (SEM) in Fig. 1a and Fig. S3 demonstrated that these carbon materials are composed of highly fused primary particles, which are sized in hundreds of nanometers and loosely packed to form secondary aggregates at the micrometer level. The morphologies of the PAC-T series are similar to each other and resemble that of parent CAV. Owing to the doping of N heteroatom, short-distance curved graphite strips are observed in the TEM image (Fig. 1b, c), and the layer spacing of the graphite strips was 0.38 nm. SEM elemental mapping images manifested a homogeneous C, N, and O distribution over the representative PAC-1100 (Fig. 1d-g). It can be seen from the XRD patterns (Fig. 2a) that all the PAC-T samples exhibited two broad diffraction peaks at $2\theta \approx 26^\circ$ and 44° , belonging to the (002) and (100)

planes for graphitized carbon, respectively [34, 35]. As the temperature increased, the peaks gradually became weaker, indicating the increased disorder degree of the graphite structure. Raman spectra (Fig. 2b) showed the two distinctive peaks 1340 (D band) and 1590 cm^{-1} (G band) relative to defective/disordered carbon and crystalline graphitic sp^2 -carbon, respectively [36-38]. The I_D/I_G values were calculated from the intensity ratio of D to G bands to quantitatively reflect the disorder degree of carbon materials. The slight increase in I_D/I_G values from 0.96 to 1.16 along with the carbonization temperatures from 800 $^{\circ}\text{C}$ to 1200 $^{\circ}\text{C}$ again suggests the formation of more defects at a higher temperature.

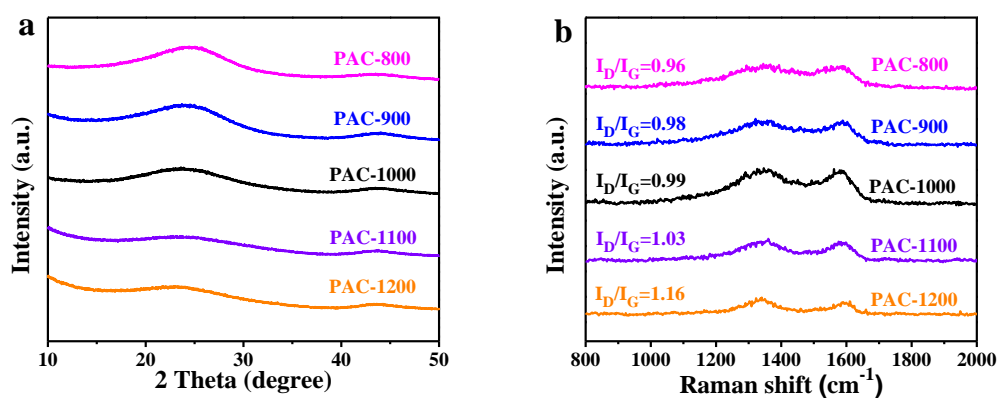


Fig. 2 (a) XRD patterns and (b) Raman spectra of PAC-T series.

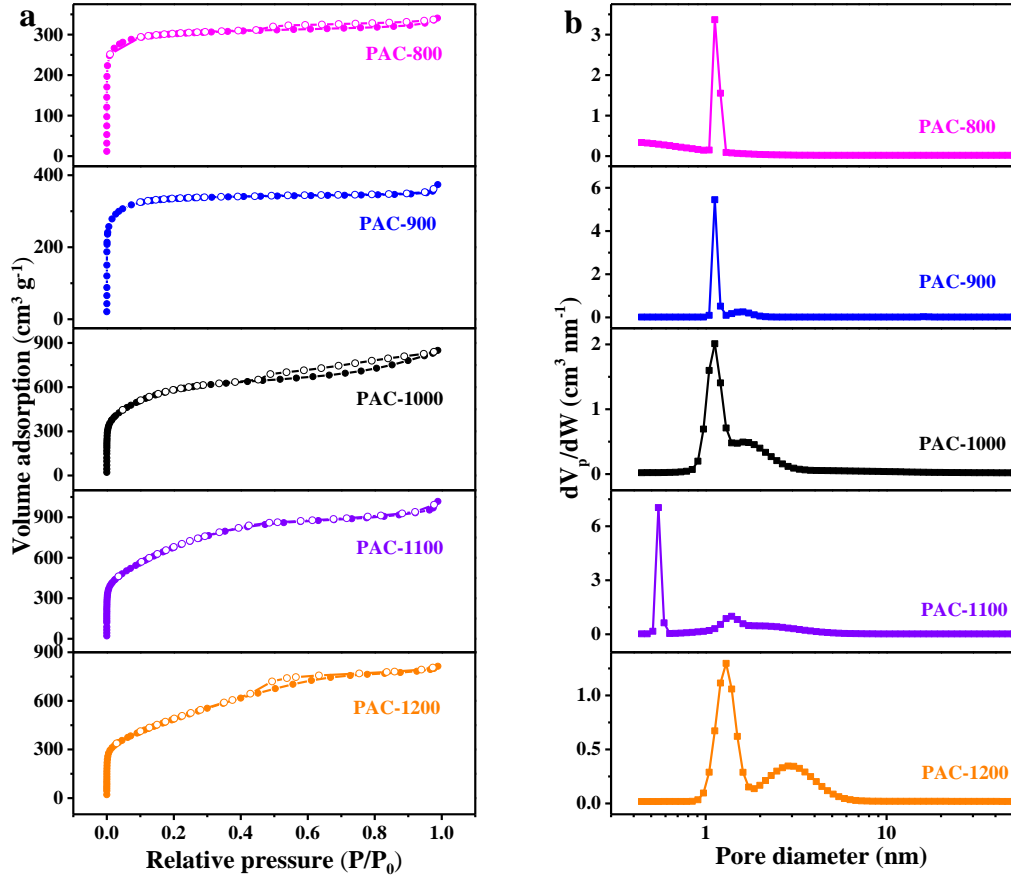


Fig. 3 (a) N_2 sorption isotherms (b) corresponding pore size distribution curves of PAC-T series.

The textural properties including the specific surface area, pore-volume, and pore size were characterized by the N_2 sorption experiment. As shown in Fig. 3a, a N_2 uptakes jump at relatively low pressure occurred in all the nitrogen sorption isotherms, reflecting the formation of a large number of micropores. Relatively weak uptakes were observed over the samples prepared at the low pyrolysis temperatures of 800 and 900 °C, and the typical type I isotherms hint the classical full microporous structure which is confirmed by the single pore-distribution in Fig. 3b. The high-temperature pyrolyzed samples (PAC-1000, PAC-1100, and PAC-1200), showed remarkably higher uptake values with the secondary enhancement at $P/P_0 > 0.4$, suggesting hierarchical pore structures [39]. Fig. 3b shows that PAC-1000 and PAC-1200 remained the similar micropore diameter to PAC-800 and PAC-900, and added the other most probable mesopores, demonstrating the hierarchically micro-/meso-pore structure. Interestingly,

PAC-1100 gave the smaller micropore at 0.5~0.6 nm, with the appearance of the other large micropore at 1~2 nm also called ultra-micropore, demonstrating an unusual bimicro-sized hierarchical pore structure. Further, among all the samples, PAC-1100 owned the maximum surface area ($2257 \text{ m}^2 \text{ g}^{-1}$) and pore volume ($1.57 \text{ cm}^3 \text{ g}^{-1}$), associating well to its plenty of small micropores and hierarchical pore structure (Table S1).

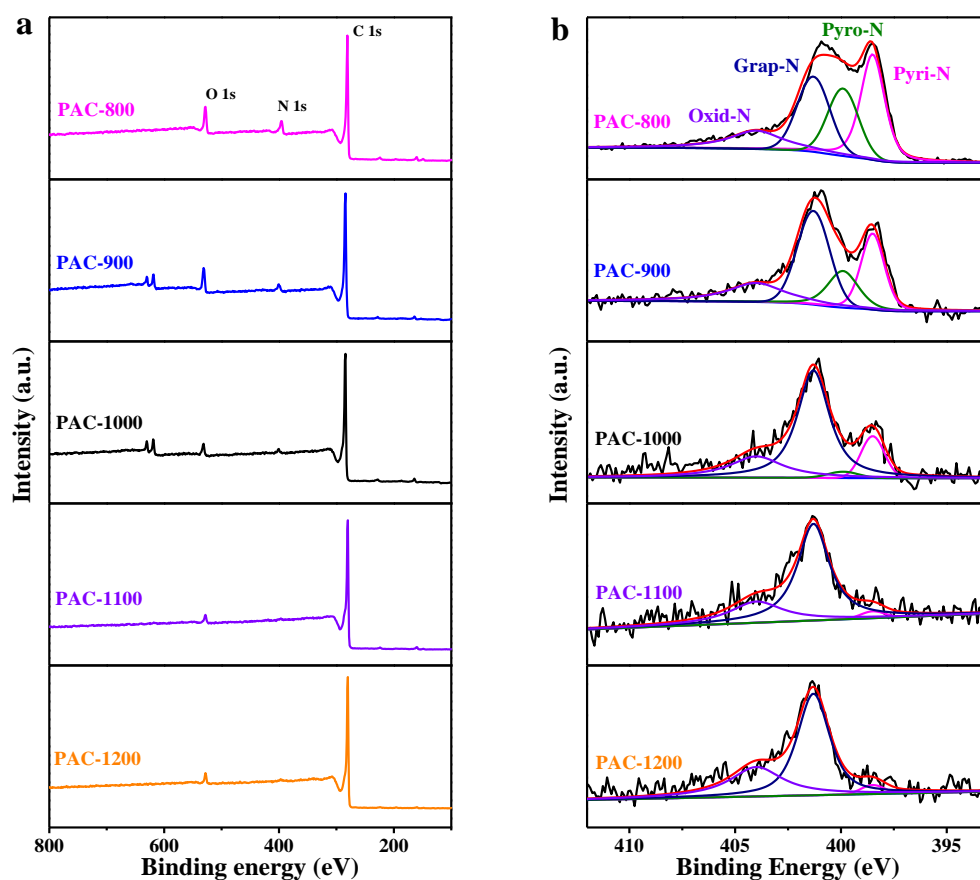


Fig. 4 (a) Survey scan XPS spectra, and (d) High-resolution N 1s XPS spectra of PAC-T series.

The C, H, N elemental compositions of CAV and PAC-T series were measured (Table S2), showing that the elemental composition of CAV was C 38.7%, N 8.1%, and H 6.2% (entry 1). After pyrolysis, the C content of PAC-T samples increased while the N contents decreased, attributable to the preferential decomposition of the heteroatomic N-containing functional groups at high temperatures. The surface chemical composition and electronic state were analyzed by X-ray photoelectron spectroscopy

(XPS) (Fig. 4a and b). The survey scan XPS spectra (Fig. 4a) displayed the signals of C, N, and O elements for all the samples. The high-resolution N1s XPS spectra (Fig. 4b) were deconvoluted into the four peaks at 398.5, 399.9, 401.3, and 404.0 eV assigned to pyridinic N (Pyri-N), pyrrolic N (Pyro-N), graphitic N (Grap-N), and oxidized N (Oxid-N), respectively [40, 41]. The high-content N species are Pyri-N and Pyro-N at the low pyrolysis temperatures of 800 and 900 °C (Table S3). Consequently, the degree of graphitization is insufficient in that case, and N atoms are distributed at the edges and fractures of the carbon layer to yield a large amount of Pyri-N and Pyro-N. Higher temperatures lead to the partial removal of N atoms and promote the re-embedding of the preserved N atoms into the carbon layer. As a result, when the pyrolysis was conducted at 1000 °C and above, Grap-N became dominating the N species, which was beyond 62% into a more stable Grap-N. PAC-1100 exhibited the highest Grap-N content of 71.0%, but the extremely high pyrolysis temperature 1200 °C caused a jump of Oxid-N with a reversely lowered Grap-N down to 62.8%. The results indicate that 1100 °C is an optimal pyrolysis temperature to obtain a sufficiently graphitized carbon material from the CAV precursor.

For comparison, self-polymerization of IL monomer [AVIM]Cl in the absence of template (P123) was carried out under the otherwise same conditions as those of CAV, giving a nonporous PIL material. Carbonization of this PIL at 1100 °C reached a control sample ⁿPAC-1100. Compared with PAC-1100, ⁿPAC-1100 exhibited a lower surface area (1680 m² g⁻¹) and pore volume (0.58 cm³ g⁻¹) (Table S1). Its nitrogen sorption isotherm was the typical type I for microporous materials (Fig. S4). Only slight increasing uptake at high relative pressure above 0.5 was observed, suggesting negligible mesopores. Clearly, the porosity of ⁿPAC-1100 is in contrast to the hierarchically porous structure of the soft template-derived PAC-1100. As

demonstrated previously, removing the soft template from the as-synthesized poly(ionic liquid) by using a solvent is difficult [33], which, however, is unnecessary in preparing carbon materials by the present pyrolysis. The above comparison indicates that the template-containing PIL material is favorable for the formation of hierarchically porous carbon, mostly due to the lower decomposing temperature of the polymeric soft template over the PIL backbone. Elemental and XPS analysis of ^{nt}PAC-1100 demonstrated that its total N content and surface chemical status of the four N species are comparable to those of PAC-1100, implying that the modulation of N species should have not been affected by the inclusion of the soft template (Fig. S5). Thus, the soft template-containing PIL acts as an interesting precursor that provides an opportunity to control the hierarchical pore formation while featuring the inherently created surface chemical state of N species.

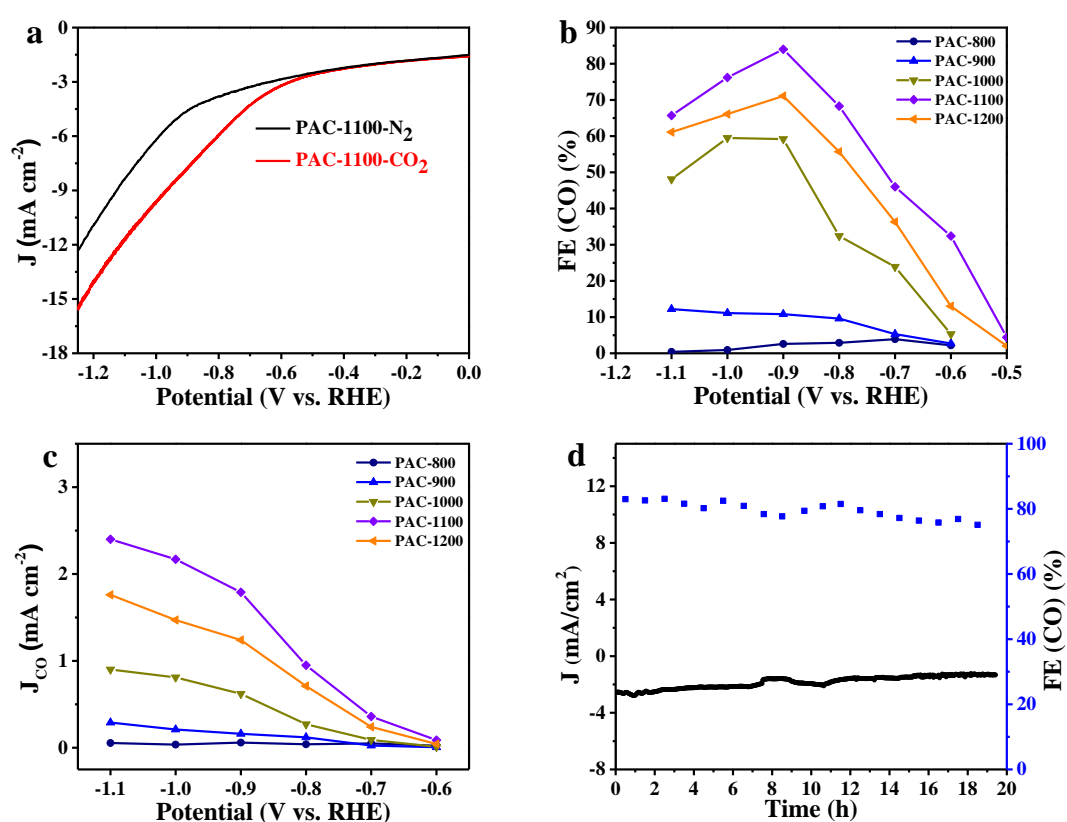


Fig. 5 Catalytic CO₂RR performance. (a) LSV curves of PAC-1100 measured in N₂- and CO₂-saturated electrolyte (0.1 mol L⁻¹ KHCO₃ solution) with a scan rate of 5 mV s⁻¹. Faraday efficiency

of (b) CO and (c) CO partial current densities of PAC-T series. (d) Stability tests of PAC-1100 at –1.5 V vs. RHE in CO₂ saturated electrolyte (0.1 mol L⁻¹ KHCO₃ solution).

3.2 Electrochemical CO₂ reduction

The CO₂RR on PAC-T series was assessed in an H-type cell by using a three-electrode system. In linear sweep voltammetry (LSV) curves of PAC-1100 with N₂ saturated 0.1 mol L⁻¹ KHCO₃ electrolyte (Fig. 5a), the onset potential was -0.9 V, implying a strong ability to inhibit hydrogen evolution reduction (HER). By contrast with CO₂ saturated electrolyte, the onset potential positively shifted to the lower region and apparently larger current density was observed, indicating the taking place of CO₂ reduction.

The CO₂RR on PAC-T series was further measured in the cathode potential range of -0.5 to -1.1 V. CO and H₂ turned out to be the main reduction products with the total Faradaic efficiencies (FEs) of around 100% and no liquid product was detected by ¹H NMR (Fig. S6). Fig 5b and Fig. S7 respectively illustrate FE (CO) (FE of CO) and FE (H₂) (FE of H₂) over PAC-T series for CO₂RR at the applied potentials. PAC-1100 showed the FE (CO) of 4.4% at the low potential of -0.5 V, which gradually increased with increasing the potential, reaching the maximum of 83.0% at -0.9 V. Further increasing the potential caused the declining of FE(CO) but dramatically enhancing of FE (H₂), indicating that HER dominated the reduction at the high potential. The phenomena allow a facile alteration of the CO/H₂ ratio to selective produce CO or syngas *via* controlling the applied potential. A similar trend was observed over other PAC-T samples. PAC-1100 exhibited the highest FE (CO) at all the employed potentials. Compared with PAC-1100 exhibiting the maximum FE (CO) of 83.0% at the potential of -0.9 V, PAC-800, PAC-900, PAC-1000, and PAC-1200 showed the FE (CO) of 3.9%, 12.2%, 59.5%, and 71.1%, respectively. Clearly, the FE (CO) gradually increased along with the pyrolysis temperature, reaching the maximum value at 1100 °C and then

decreasing at the higher temperature. Fig. 5c shows the CO partial current density J_{CO} , (normalized by the geometrical surface area) on PAC-T series against the applied potential. PAC-1100 displayed the largest J_{CO} in the entire applied potential range, reflecting the fastest reaction kinetics in CO₂RR. The J_{CO} on PAC-800 was nearly zero, in line with its sluggish catalytic performance in CO₂RR at the low pyrolysis temperature. Along with the increase of pyrolysis temperature, PAC-1100 afforded the J_{CO} of 1.79 mA cm⁻² at the potential of -0.9 V, again reflecting the efficiency in tuning the CO₂RR activity by manipulating the pyrolysis temperature. A long-term CO₂RR performance on PAC-1100 was carried out at the constant cathode potential of -0.9 V vs. RHE (Fig. 5d). Only a slight decay of FE (CO) and J_{CO} was observed in the initial stage, after which they became quite stable up to 20 h.

For comparison, CO₂RR over ^mPAC-1100 was evaluated in potentials from -0.6 to -1.0 V vs. RHE. The maximum FE (CO) of 61.2% with the J_{CO} 0.76 mA cm⁻² at the potential of -0.9 V vs. RHE were much lower than those on PAC-1100. The comparison visualizes the advantage of the utilization of porous PIL as the carbon precursor for CO₂RR (Fig. S7).

To ascertain the CO production from CO₂RR process rather than the reduction of KHCO₃ or the decomposition of catalysts, potentiostat electrolysis on PAC-1100 was performed in N₂ saturated 0.1 mol L⁻¹ KHCO₃ electrolyte at -0.9 V vs. RHE (Fig. S8). When the CO₂ saturated electrolyte was replaced by N₂ saturated one, FE (CO) dropped from 83.0% to 1.1% with the main product of H₂, confirming the origination of CO from CO₂ reduction. Further, H₂ formation with negligible FE (CO) was found for the electrolysis on carbon paper in CO₂ saturated 0.1 mol L⁻¹ KHCO₃ electrolyte, emphasizing the key role of electrocatalyst PAC-1100 (Fig. S9).

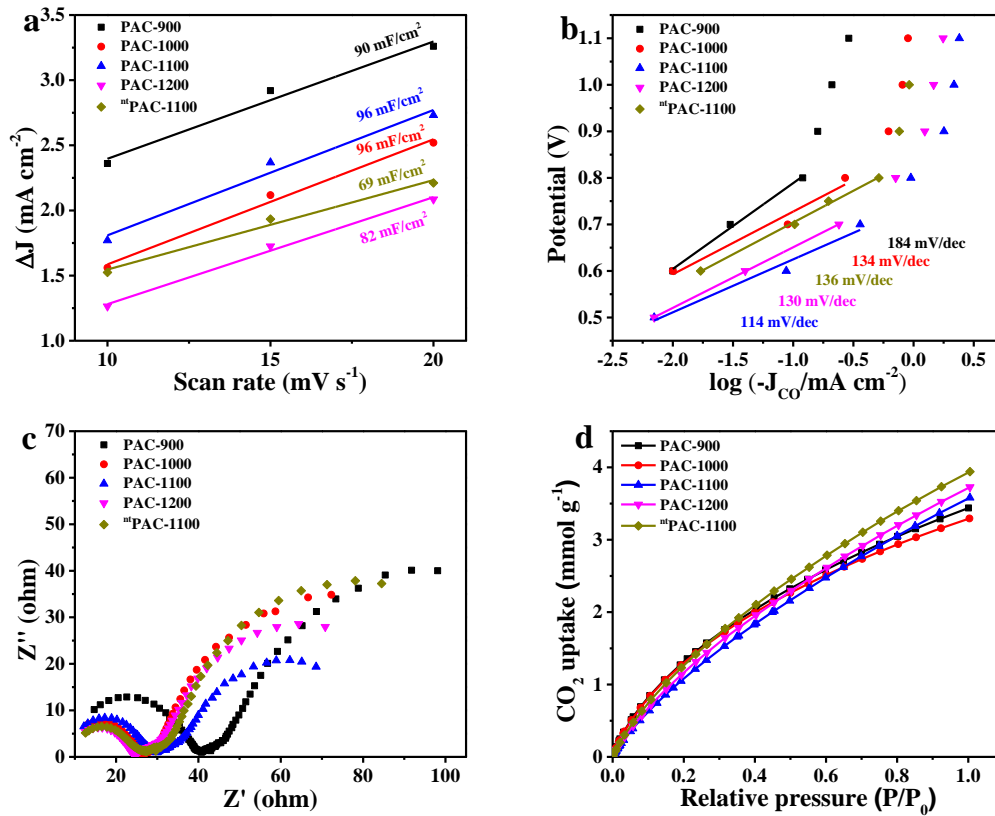


Fig. 6 (a) double-layer capacitance, (b) Tafel plots for CO formation, (c) EIS at -1.5 V vs RHE, and (d) CO_2 adsorption isotherms of PAC-900, PAC-1000, PAC-1100, PAC-1200, and $^n\text{PAC-1100}$ at 298 K.

3.3 Understanding of electrocatalysis performance

For CO_2RR , neat carbon has been reported to be inactive, while the content and type of N dopant play a crucial role in the action [42]. For PAC-T of this work, the variation of the maximum FE (CO) resembles that of Grap-N content, whereas no such regulation is required for Pyri-N, Pyro-N, and Oxid-N (Fig. S10a). On the one hand, Grap-N plays a positive role in improving the conductivity of carbon materials. On the other hand, it shows a strong affinity towards the key intermediate $^*\text{CO}_2^-$ such that the energy barrier is lowered and the activity is enhanced [43, 44]. Further, the exposure and accessibility of the N active sites is another key factor to influence the CO_2RR performance [42, 45]. The variation of the maximum FE (CO) on PAC-T series is similar to that of the specific surface area (Fig. S10b), where PAC-1100 with the highest specific surface area

possessed the best FE (CO). This relationship is confirmed by the comparison of PAC-1100 with ^mPAC-1100; both of them owned more or less similar surface chemical states but the latter with lower specific surface area was less active.

In order to more comprehensively interpret the importance of the exposure and accessibility of active sites, the electrochemical surface area (ECSA) is calculated from the double-layer capacitance (C_{dl}) by collecting the cyclic voltammograms (CV) curves at varied scanning rate (Fig. S11). For PAC-900, the ECSA value was as high as 90 mF cm⁻², attributable to the high total N content though with a low specific surface area. With increasing pyrolysis temperature, the higher ECSA of 96 mF cm⁻² was observed for PAC-1000 and PAC-1100, a compromised result of increase of specific surface area and decrease of N content. Further raising the pyrolysis temperature up to 1200 °C caused a drop ECSA down to 82 mF cm⁻² due to reducing the specific surface area and N content. Besides, ^mPAC-1100 only showed the ECSA 69 mF cm⁻² mainly because of its very small specific surface area. It is thus rational that the best CO₂RR activity of PAC-1100 should associate with its most abundant Grap-N species, as well as the highest specific and electrochemical surface areas that suggest good exposure and ready accessibility of these active sites (Fig. 6a).

The electrocatalytic kinetics of various catalysts in CO₂RR process were evaluated by Tafel slopes, which were calculated by linearly plotting the overpotential vs. $\log J_{CO}$ (logarithm of J_{CO}) in the initial low overpotential range (Fig. 6b). PAC-1100 exhibited a Tafel slope of 114 mV dec⁻¹, very close to the theoretical value of 118 mV dec⁻¹ with the rate-determining step of the initial transfer of one electron to CO₂ to form surface adsorbed *CO₂⁻ intermediate [45]. The Tafel slope of PAC-1100 is higher than those of other PAC-T members. These data suggest the fastest catalytic kinetics of PAC-1100. Moreover, the electrochemical impedance spectroscopy (EIS) of these samples was

measured at the overpotential of -0.9 V vs. RHE (Fig. 6c). In a Nyquist diagram, the first semicircle diameter represents the ohmic resistance for internal conductivity, and the second one represents the interface charge transfer resistance, the charge transfer resistance between the catalyst and reactant/intermediate, reflecting the diffusion rate, adsorption of reactants, and desorption of products. As shown in Fig. 6c, PAC-900 had an apparently large radius of the first semicircle, revealing the poor inherent conductivity due to the inferior graphitization. The small radius of the first semicircles were observable for other samples, index of favorable conductivity. The sequence of the second semicircle is identical to their CO₂RR activity, with PAC-1100 offering the smallest radius, indicative of the lowest interface charge transfer resistance. This EIS observation on PAC-1100 is also advantageous for promoting its reaction kinetic, in good agreement with the above Tafel slopes result [37].

As revealed above, the fast kinetics and high activity of PAC-1100 could be tentatively ascribed to plenty of Grap-N sites with good exposure and readily accessibility. Thus, it seems that the champion catalyst should have the best CO₂ adsorption capability [46]. Nonetheless, PAC-1100 did not show the highest CO₂ uptake among PAC-T series measured by the adsorption isotherms at 298K (Fig. 6d). When fitted with a double-site Langmuir (DL) model, two types of sites were demonstrated over PAC-T for capturing CO₂ (Fig. S12): weak and strong adsorption sites. With the elevation of pyrolysis temperature, the saturated CO₂ uptake on the abundant weak adsorption sites (q_c) gradually increased, accompanied by the decrease of the equilibrium constant k_c (affinity coefficient of the weak site). Meanwhile, a reverse trend was found for the strong adsorption sites (q_i and k_i). This is understandable because the high-temperature pyrolysis reduces the content of N species for strong adsorption sites but greatly increases the specific surface area bearing larger amounts

of weak sorption sites. Owing to the combined effects of the two sites, all of the PAC-T samples exhibited considerably high CO₂ uptakes [47]. Particularly, ^mPAC-1100 showed similar CO₂ adsorption isotherms and DL parameters to those of PAC-1100, though the former possessed a much lower specific surface area. Previous reports have shown that, in addition to the specific surface area, hierarchically porous structures for N-doped carbon materials were more crucial for CO₂RR, in which large pores improved mass transfer and small pores benefited CO₂ enrichment nearby the N active sites [48]. It is interesting to note the unusual small-/ultra-microporous hierarchical structure for PAC-1100, whereas its analogs owned more popular micro-/meso-porous hierarchical structures. The small-micropore size of PAC-1100 is 0.5~0.6 nm, slightly larger than the dynamic diameter of CO₂ molecule. In this case, the nano-confinement effect is remarkable, increasing the collision probability of CO₂ molecule with pore wall accommodating the active sites. This small-micropore confinement effect is unique for PAC-1100, and plays an exclusively positive role in improving the CO₂RR reactivity.

4. Conclusions

A series of N-doped porous carbon materials was prepared by pyrolysis of the soft template-containing poly(ionic liquid) precursor, which was synthesized by free radical self-polymerization of an ionic liquid monomer in the presence the soft-template P123. By adjusting pyrolysis temperatures, porosity and N species were modulated for the carbon materials; the pyrolysis at 1100 °C afforded the champion sample PAC-1100 with the maximum specific surface area and graphic N content, as well as the unique hierarchically small-/ultra-microporous structure. PAC-1100 was effective in the CO₂RR into CO, exhibiting considerably high Faraday efficiency and current density plus well duration. The identification of the structure-performance relationship suggests that the graphic N species played a vital role in the CO₂RR process. The abundant

porosity and graphitic N species were observed to promote the activity by facilitating the kinetics and providing a large electrochemical surface area. Specifically, the unique hierarchically small-/ultra-micropore was crucial for the high activity: the ultra-micropore promoted mass transfer while the small-micropore of 0.5~0.6 nm enhanced the reactivity of CO₂ through the nano-confinement effect. This work fabricates the first example of soft template-containing PIL-derived hierarchically N-doped porous carbon material for CO₂RR towards CO and highlights the importance of the internal porosity of the precursor in controlling the structure and function of the carbon materials.

Acknowledgments

This work was supported by the National Natural Science Foundation of China (Nos. 22072065, U1662107, and 21476109), Six talent peaks project in Jiangsu Province (JNHB-035), State Key Laboratory of Materials-Oriented Chemical Engineering (KL17-04), and the Project of Priority Academic Program Development of Jiangsu Higher Education Institutions (PAPD).

References

- [1] J. Wu, T. Sharifi, Y. Gao, T. Zhang, P.M. Ajayan, Emerging carbon-based heterogeneous catalysts for electrochemical reduction of carbon dioxide into value-added chemicals, *Adv. Mater.* 31 (2019) 1804257-1804280.
- [2] P. Prabhu, V. Jose, J.-M. Lee, Heterostructured catalysts for electrocatalytic and photocatalytic carbon dioxide reduction, *Adv. Funct. Mater.* 30 (2020) 1910768-1910799.
- [3] X. Duan, J. Xu, Z. Wei, J. Ma, S. Guo, S. Wang, H. Liu, S. Dou, Metal-free carbon materials for CO₂ electrochemical reduction, *Adv. Mater.* 29 (2017) 1701784-1701803.
- [4] D. Esrafilzadeh, A. Zavabeti, R. Jalili, P. Atkin, J. Choi, B.J. Carey, R. Brkljaca,

A.P. O'Mullane, M.D. Dickey, D.L. Officer, D.R. MacFarlane, T. Daeneke, K. Kalantar-Zadeh, Room temperature CO₂ reduction to solid carbon species on liquid metals featuring atomically thin ceria interfaces, *Nat. Commun.* 10 (2019) 865.

[5] A. Sofia Varela, W. Ju, P. Strasser, Molecular nitrogen-carbon catalysts, solid metal organic framework catalysts, and solid metal/nitrogen-doped carbon (MNC) catalysts for the electrochemical CO₂ reduction, *Adv. Energy Mater.* 8 (2018) 1703614-1703648.

[6] J. Gu, C.-S. Hsu, L. Bai, H.M. Chen, X. Hu, Atomically dispersed Fe³⁺ sites catalyze efficient CO₂ electroreduction to CO, *Science*. 364 (2019) 1091-1094.

[7] D. Yang, Q. Zhu, C. Chen, H. Liu, Z. Liu, Z. Zhao, X. Zhang, S. Liu, B. Han, Selective electroreduction of carbon dioxide to methanol on copper selenide nanocatalysts, *Nat. Commun.* 10 (2019) 677.

[8] M. Liu, Y. Pang, B. Zhang, P. De Luna, O. Voznyy, J. Xu, X. Zheng, C.T. Dinh, F. Fan, C. Cao, F.P.G. de Arquer, T.S. Safaei, A. Mepham, A. Klinkova, E. Kumacheva, T. Filleter, D. Sinton, S.O. Kelley, E.H. Sargent, Enhanced electrocatalytic CO₂ reduction via field-induced reagent concentration, *Nature*. 537 (2016) 382-386.

[9] S. Zhu, X. Qin, Q. Wang, T. Li, R. Tao, M. Gu, M. Shao, Composition-dependent CO₂ electrochemical reduction activity and selectivity on Au-Pd core-shell nanoparticles, *J. Mater. Chem. A*, 7 (2019) 16954-16961.

[10] S.C. Abeyweera, J. Yu, J.P. Perdew, Q. Yan, Y. Sun, Hierarchically 3D porous Ag nanostructures derived from silver benzenethiolate nanoboxes: Enabling CO₂ reduction with a near-unity selectivity and mass-specific current density over 500 A/g, *Nano Lett.* 20 (2020) 2806-2811.

- [11] X. Zhu, J.-H. Liu, X.-S. Li, J.-L. Liu, X. Qu, A.-M. Zhu, Enhanced effect of plasma on catalytic reduction of CO₂ to CO with hydrogen over Au/CeO₂ at low temperature, *J. Energy Chem.* 26 (2017) 488-493.
- [12] T. Liu, S. Ali, Z. Lian, B. Li, D.S. Su, CO₂ electroreduction reaction on heteroatom-doped carbon cathode materials, *J. Mater. Chem. A.* 5 (2017) 21596-21603.
- [13] J. Xie, X. Zhao, M. Wu, Q. Li, Y. Wang, J. Yao, Metal-free fluorine-doped carbon electrocatalyst for CO₂ reduction outcompeting hydrogen evolution, *Angew. Chem. Int. Ed.* 57 (2018) 9640-9644.
- [14] S. Mou, T. Wu, J. Xie, Y. Zhang, L. Ji, H. Huang, T. Wang, Y. Luo, X. Xiong, B. Tang, X. Sun, Boron phosphide nanoparticles: A nonmetal catalyst for high-selectivity electrochemical reduction of CO₂ to CH₃OH, *Adv. Mater.* 31 (2019) 1903499-1903504.
- [15] S. Schlager, L.M. Dumitru, M. Haberbauer, A. Fuchsbauer, H. Neugebauer, D. Hiemetsberger, A. Wagner, E. Portenkirchner, N.S. Sariciftci, Electrochemical reduction of carbon dioxide to methanol by direct injection of electrons into immobilized enzymes on a modified electrode, *ChemSusChem*, 9 (2016) 631-635.
- [16] T. Benedetti, S. Naficy, A. Walker, D.L. Officer, G.G. Wallace, F. Dehghani, Solid-state poly(ionic liquid) gels for simultaneous CO₂ adsorption and electrochemical reduction, *Energy Technol.* 6 (2018) 702-709.
- [17] N. Sreekanth, M.A. Nazrulla, T.V. Vineesh, K. Sailaja, K.L. Phani, Metal-free boron-doped graphene for selective electroreduction of carbon dioxide to formic acid/formate, *Chem. Commun.* 51 (2015) 16061-16064.
- [18] Y. Song, W. Chen, C. Zhao, S. Li, W. Wei, Y. Sun, Metal-free nitrogen-doped

mesoporous carbon for electroreduction of CO₂ to ethanol, *Angew. Chem. Int. Ed.* 56 (2017) 10840-10844.

[19] T. Liu, S. Ali, Z. Lian, C. Si, D.S. Su, B. Li, Phosphorus-doped onion-like carbon for CO₂ electrochemical reduction: the decisive role of the bonding configuration of phosphorus, *J. Mater. Chem. A.* 6 (2018) 19998-20004.

[20] S. Liu, H. Yang, X. Su, J. Ding, Q. Mao, Y. Huang, T. Zhang, B. Liu, Rational design of carbon-based metal-free catalysts for electrochemical carbon dioxide reduction: A review, *J. Energy Chem.* 36 (2019) 95-105.

[21] K. Miura, J. Hayashi, K. Hashimoto, Production of molecular-sieving carbon through carbonization of coal modified by organic additives, *Carbon.* 29 (1991) 653-660.

[22] Z.X. Ma, T. Kyotani, Z. Liu, O. Terasaki, A. Tomita, Very high surface area microporous carbon with a three-dimensional nano-array structure: Synthesis and its molecular structure, *Chem. Mater.* 13 (2001) 4413-4415.

[23] M. Chen, S. Wang, H. Zhang, P. Zhang, Z. Tian, M. Lu, X. Xie, L. Huang, W. Huang, Intrinsic defects in biomass-derived carbons facilitate electroreduction of CO₂, *Nano Res.* 13 (2020) 729-735.

[24] X. Xu, Y. Li, Y. Gong, P. Zhang, H. Li, Y. Wang, Synthesis of palladium nanoparticles supported on mesoporous N-doped carbon and their catalytic ability for biofuel upgrade, *J. Am. Chem. Soc.* 134 (2012) 16987-16990.

[25] F. Cui, Q. Deng, H. Zhao, Y. Jiang, J. Li, Ionic liquid promoted synthesis of nitrogen, phosphorus, and fluorine triple-doped mesoporous carbon as metal-free

- electrocatalyst for oxygen reduction reaction, *Ionics*. 26 (2020) 4609-4619.
- [26] J. Wang, X. Duan, J. Gao, Y. Shen, X. Feng, Z. Yu, X. Tan, S. Liu, S. Wang, Roles of structure defect, oxygen groups and heteroatom doping on carbon in nonradical oxidation of water contaminants, *Water Res.* 185 (2020) 116244.
- [27] Z. Xiao, D. Kong, J. Liang, B. Wang, R. Iqbal, Q.-H. Yang, L. Zhi, Structure controllable carbon matrix derived from benzene-constructed porous organic polymers for high-performance Li-S batteries, *Carbon*. 116 (2017) 633-639.
- [28] W. Zhang, S. Wei, Y. Wu, Y.-L. Wang, M. Zhang, D. Roy, H. Wang, J. Yuan, Q. Zhao, Poly(Ionic Liquid)-derived graphitic nanoporous carbon membrane enables superior supercapacitive energy storage, *ACS Nano*. 13 (2019) 10261-10271.
- [29] J. Gong, H. Lin, M. Antonietti, J. Yuan, Nitrogen-doped porous carbon nanosheets derived from poly(ionic liquid)s: hierarchical pore structures for efficient CO₂ capture and dye removal, *J. Mater. Chem. A*. 4 (2016) 7313-7321.
- [30] W. Alkarmo, F. Ouhib, A. Aqil, J.-M. Thomassin, J. Yuan, J. Gong, B. Vertruyen, C. Detrembleur, C. Jerome, Poly(ionic liquid)-derived N-doped carbons with hierarchical porosity for lithium- and sodium-ion batteries, *Macromol. Rapid Commun.* 40 (2019) 1800545-1800550.
- [31] H. Wang, J. Jia, P. Song, Q. Wang, D. Li, S. Min, C. Qian, L. Wang, Y.F. Li, C. Ma, T. Wu, J. Yuan, M. Antonietti, G.A. Ozin, Efficient electrocatalytic reduction of CO₂ by nitrogen-doped nanoporous carbon/carbon nanotube membranes: A step towards the electrochemical CO₂ refinery, *Angew. Chem. Int. Ed.* 56 (2017) 7847-7852.
- [32] J. Gao, C. He, J. Liu, P. Ren, H. Lu, J. Feng, Z. Zou, Z. Yin, X. Wen, X. Tan,

Polymerizable ionic liquid as a precursor for N, P co-doped carbon toward the oxygen reduction reaction, *Catal. Sci. Technol.* 8 (2018) 1142-1150.

[33] C. Gao, G. Chen, X. Wang, J. Li, Y. Zhou, J. Wang, A hierarchical meso-macroporous poly(ionic liquid) monolith derived from a single soft template, *Chem. Commun.* 51 (2015) 4969-4972.

[34] A.V. Korobeinyk, R.L.D. Whitby, S.V. Mikhalovsky, High temperature oxidative resistance of polyacrylonitrile-methylmethacrylate copolymer powder converting to a carbonized monolith, *Eur. Polym. J.* 48 (2012) 97-104.

[35] C. Chen, X. Sun, X. Yan, Y. Wu, H. Liu, Q. Zhu, B.B.A. Bediako, B. Han, Boosting CO₂ electroreduction on N,P-co-doped carbon aerogels, *Angew. Chem. Int. Ed.* 59 (2020) 11123-11129.

[36] C. Li, Y. Wang, N. Xiao, H. Li, Y. Ji, Z. Guo, C. Liu, J. Qiu, Nitrogen-doped porous carbon from coal for high efficiency CO₂ electrocatalytic reduction, *Carbon.* 151 (2019) 46-52.

[37] F. Pan, B. Li, W. Deng, Z. Du, Y. Gang, G. Wang, Y. Li, Promoting electrocatalytic CO₂ reduction on nitrogen-doped carbon with sulfur addition, *Appl.Catal. B-Environ.* 252 (2019) 240-249.

[38] W. Liu, J. Qi, P. Bai, W. Zhang, L. Xu, Utilizing spatial confinement effect of N atoms in micropores of coal-based metal-free material for efficiently electrochemical reduction of carbon dioxide, *Appl.Catal. B-Environ.* 272 (2020) 118974-118982.

[39] H. Pan, Z.B. Cheng, Z.B. Xiao, X.J. Li, R.H. Wang, The fusion of imidazolium-based ionic polymer and carbon nanotubes: One type of new heteroatom-doped carbon

precursors for high-performance lithium-sulfur batteries, *Adv. Funct. Mater.* 27 (2017) 1703936-1703946.

[40] P. Su, K. Iwase, S. Nakanishi, K. Hashimoto, K. Kamiya, Nickel-nitrogen-modified graphene: An efficient electrocatalyst for the reduction of carbon dioxide to carbon monoxide, *Small*. 12 (2016) 6083-6089.

[41] F. Pan, B. Li, X. Xiang, G. Wang, Y. Li, Efficient CO₂ electroreduction by highly dense and active pyridinic nitrogen on holey carbon layers with fluorine engineering, *ACS Catal.* 9 (2019) 2124-2133.

[42] P.P. Sharma, J. Wu, R.M. Yadav, M. Liu, C.J. Wright, C.S. Tiwary, B.I. Yakobson, J. Lou, P.M. Ajayan, X.-D. Zhou, Nitrogen-doped carbon nanotube arrays for high-efficiency electrochemical reduction of CO₂: On the understanding of defects, defect density, and selectivity, *Angew. Chem. Int. Ed.* 54 (2015) 13701-13705.

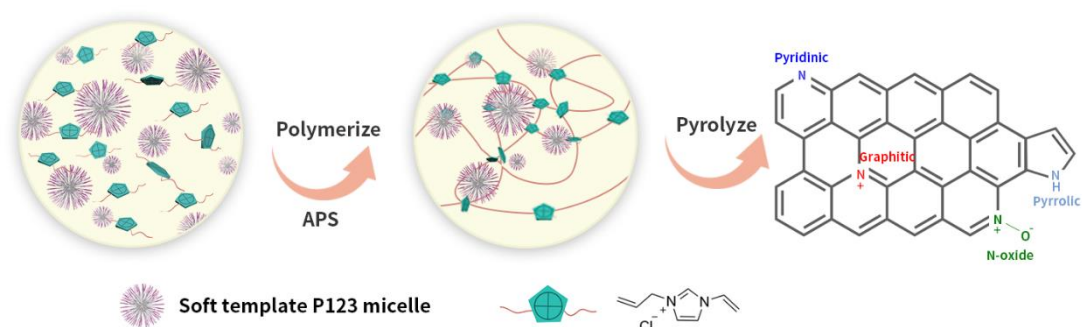
[43] G.-L. Chai, Z.-X. Guo, Highly effective sites and selectivity of nitrogen-doped graphene/CNT catalysts for CO₂ electrochemical reduction, *Chem. Sci.* 7 (2016) 1268-1275.

[44] J. Xu, Y. Kan, R. Huang, B. Zhang, B. Wang, K.-H. Wu, Y. Lin, X. Sun, Q. Li, G. Centi, D. Su, Revealing the origin of activity in nitrogen-doped nanocarbons towards electrocatalytic reduction of carbon dioxide, *ChemSusChem*. 9 (2016) 1085-1089.

[45] H. Yang, Y. Wu, Q. Lin, L. Fan, X. Chai, Q. Zhang, J. Liu, C. He, Z. Lin, Composition tailoring via N and S co-doping and structure tuning by constructing hierarchical pores: Metal-free catalysts for high-performance electrochemical reduction of CO₂, *Angew. Chem. Int. Ed.* 57 (2018) 15476-15480.

- [46] H. Wang, H. Wang, G. Liu, Q. Yan, In-situ pyrolysis of taihu blue algae biomass as appealing porous carbon adsorbent for CO₂ capture: Role of the intrinsic N, *Sci. Total. Environ.* 771 (2021) 145424-145424.
- [47] J. Song, W. Shen, J. Wang, W. Fan, Superior carbon-based CO₂ adsorbents prepared from poplar anthers, *Carbon.* 69 (2014) 255-263.
- [48] P. Yao, T. Li, Y. Qiu, Q. Zheng, H. Zhang, J. Yan, X. Li, N-doped hierarchical porous carbon derived from bismuth salts decorated ZIF8 as a highly efficient electrocatalyst for CO₂ reduction, *J. Mater. Chem. A.* 9 (2021) 320-326.

Schemes



Scheme 1. Synthetic route of porous poly(ionic liquid) CAV and the corresponding derived carbon materials.

Figures

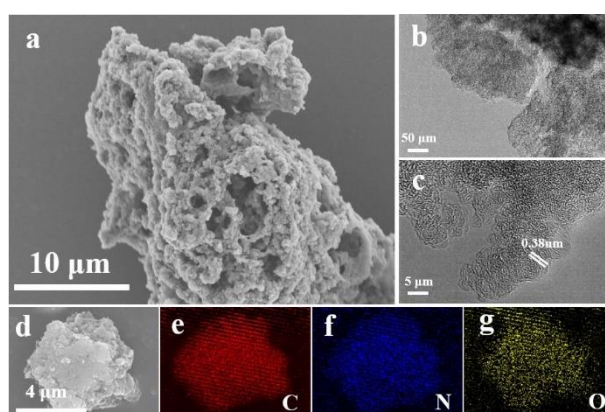


Fig. 1 (a) SEM image, (b, c) TEM images, and (d-g) SEM elemental (C, N, and O) imagings of PAC-1100.

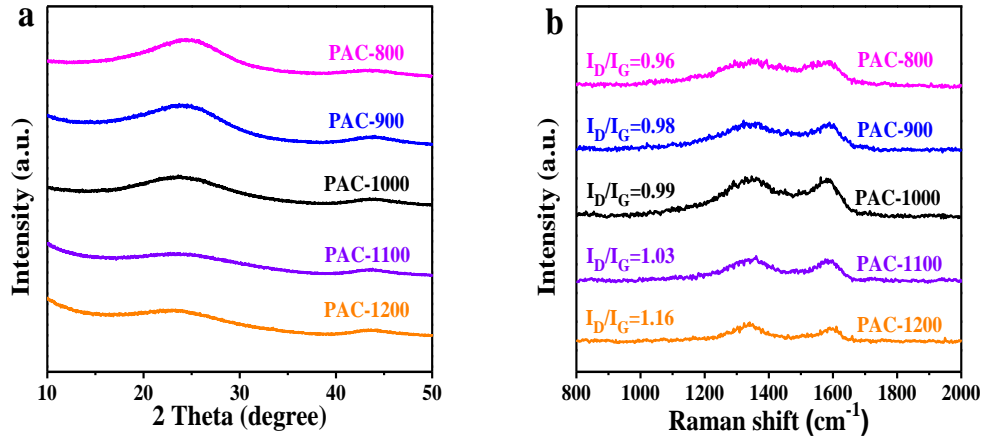


Fig. 2 (a) XRD patterns and (b) Raman spectra of PAC-T series.

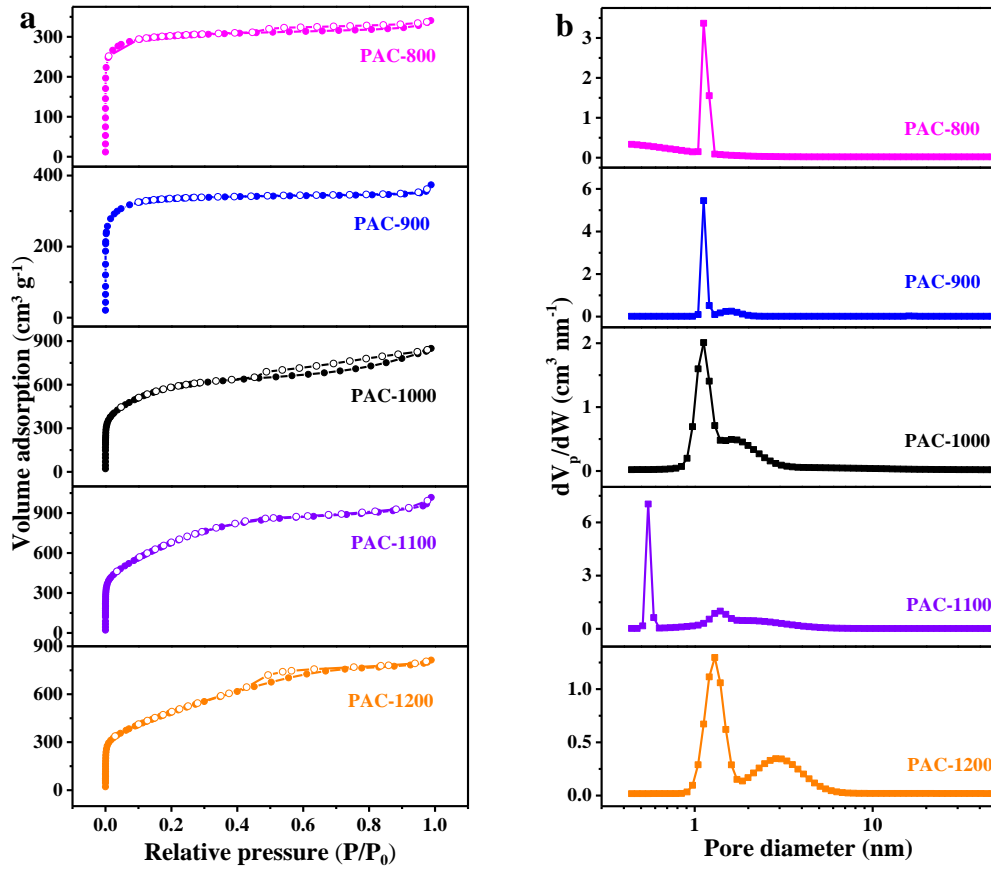


Fig. 3 (a) N₂ sorption isotherms (b) corresponding pore size distribution curves of PAC-T series.

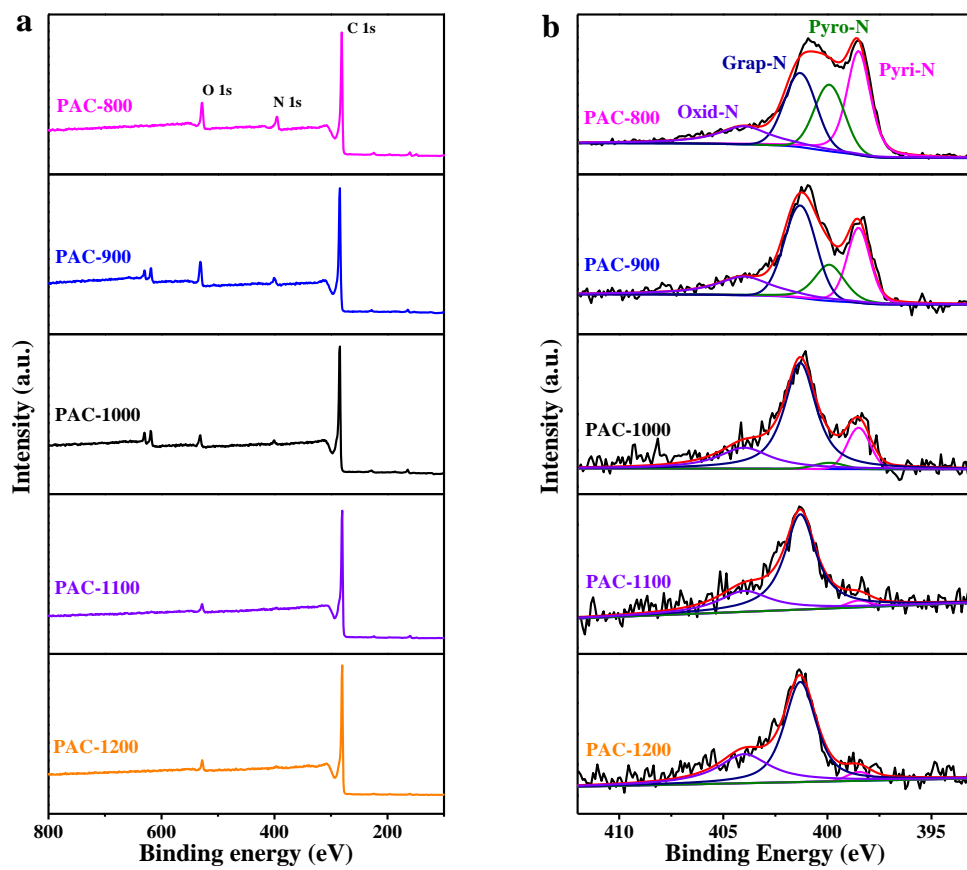


Fig. 4 (a) Survey scan XPS spectra, and (d) High-resolution N 1s XPS spectra of PAC-T series.

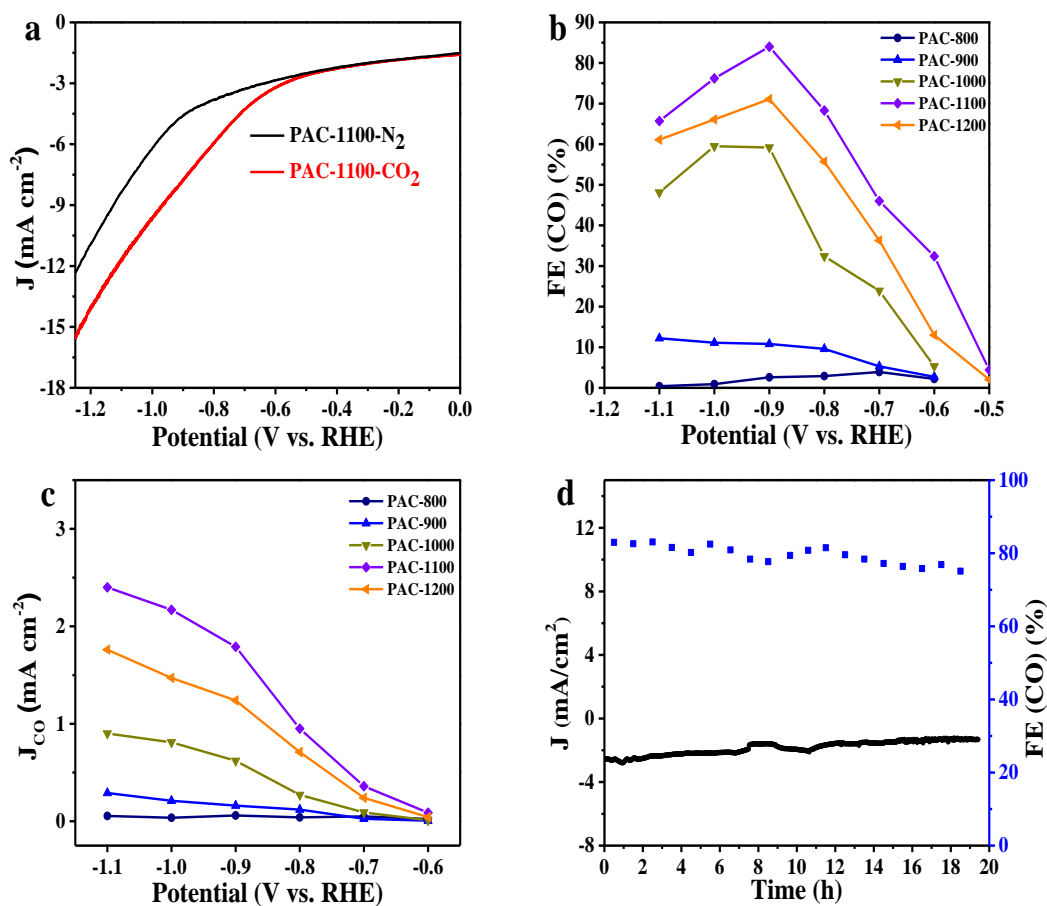


Fig. 5 Catalytic CO₂RR performance. (a) LSV curves of PAC-1100 measured in N₂- and CO₂-saturated electrolyte (0.1 M KHCO₃ solution) with a scan rate of 5 mV s⁻¹. Faraday efficiency of (b) CO and (c) CO partial current densities of PAC-T series. (d) Stability tests of PAC-1100 at -1.5 V vs. RHE in CO₂ saturated electrolyte (0.1 M KHCO₃ solution).

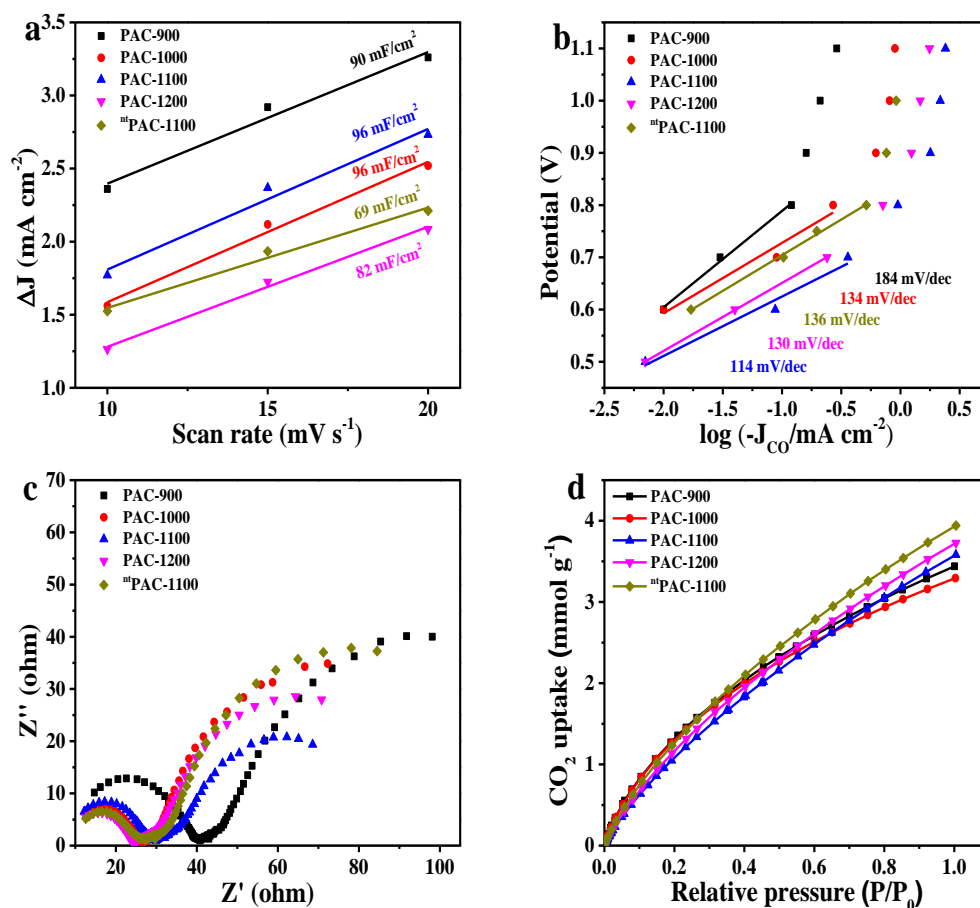


Fig. 6 (a) double-layer capacitance, (b) Tafel plots for CO formation, (c) EIS at -1.5 V vs RHE, and (d) CO₂ adsorption isotherms of PAC-900, PAC-1000, PAC-1100, PAC-1200, and ^{nt}PAC-1100 at 298.

There is not any tables in the main text of this manuscript.

Chinese Journal of Chemical Engineering

Transfer of Copyright Agreement

Scientific publishers and authors share a common interest in the protection of copyright: authors principally because they want their creative work to be protected from plagiarism and other unlawful uses, publishers because they need to protect their work and investment in the publication, marketing and distribution of the article written by the author(s) for each article being published. We therefore would like you to complete and return this form promptly, retaining a copy for your records. Your co-operation is essential and appreciated.

Article title: Pyrolyzing 5-f template-containing poly(ionic liquid) into hierarchical N-doped porous carbon for electroreduction of carbon dioxide

Author(s): Mingdong Sun, Zhengyun Bian, Weiwei Cui, Xiaolong Zhao, Shu Dong, Xuebin Ke, Yu Zhou, Jun Wang

Company or institution: Nanjing Tech University

To be published in the *Chinese Journal of Chemical Engineering*.

Effective upon acceptance for publication, copyright (including all rights thereunder and the right to obtain copyright registration in the name of the publisher, where separately or as a part of proceedings or otherwise) in the above article is hereby transferred throughout the world and for the full term and all extensions and renewals thereof, to Chemical Industry Press.

This transfer includes the right to adapt the article for use in conjunction with computer systems and programs, including reproduction or publication in machine-readable form and incorporation in retrieval systems.

Rights of authors

The publisher recognizes the retention of the following rights by the author(s):

1. Patent and trademark rights and any process or procedure described in the article.
2. The right to photocopy or make single electronic copies of the article for their own personnel use, including for their own classroom use, or for the personal use of colleagues, provided the copies are not offered for sale and are not distributed in a systematic way outside for their employing institution (e.g. via an e-mail list or public file server). Posting of the article on a secure network (not accessible to the public) within the author's institution is permitted.
3. The right, subsequently to publication, to use the article or any part thereof free of charge in a printed compilation of works of their own, such as collected writing or lecture notes.

Note

- ◆ All copies, paper or electronic or other use of the information must include an indication of

the copyright and a full citation of the proceeding source.

- ◆ Please refer requests for all uses not included above, including the authorization of other parties to reproduce or otherwise use all or part of the article (including figures and tables), to Editorial Office of Chinese Journal of Chemical Engineering

Authorship

If the article was prepared jointly with author(s), the signing author has informed the coauthor(s) of the terms of this copyright transfer and is signing on their behalf as their agent and represents that he or she is authorized to do so. Please confirm by ticking the appropriate item following the signature line. The signing author shall bear responsibility for designating the coauthor(s) and must inform the publisher of any changes in authorship.

If copyright is held by the employer, the employer or an authorized representative of the employer must sign. If the author signs, it is understood that this is with the authorization of the employer and the employer's acceptance of the terms of the transfer. Please confirm by ticking the appropriate item following the signature line.

Warranties

The author(s) warrant(s) that the article is the author's original work and has not been submitted or published elsewhere. The author(s) warrant(s) that the article contains no libelous or other unlawful statements, and does not infringe on the rights of others. If except from copyright works are included, the author(s) has (have) obtained or will obtain written permission from the copyrights owners and will credit the sources in the article.

Preprints

The author(s) must agree that if a prior version of this work (normally a preprint) has been posted to an electric public server, they will not update and/or replace the prior version in order to make it identical in contents to the final published version.

First author signature: Mingdong Sun

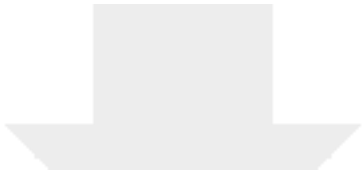
Corresponding author signature: Jun Wang E-mail address: junwang@njtech.edu.cn

Co-contributor's signature: Zhengyun Bian, Weiwei Cui, Xiaolong Zhao, Shu Dong, Xuebin Ke

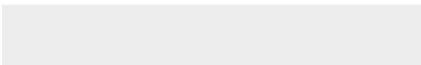
Date: March 11, 2021

Please sign the copyright agreement in person, and submit an electronic scanned copy online.

< =;ð\ ýSupplementaryPlaceholder R ýý Eílé



Click here to access/download
Supplementary Material
ESI.doc



Declaration of interests

The authors declare that they have no known competing financial interests or personal relationships that could have appeared to influence the work reported in this paper.

The authors declare the following financial interests/personal relationships which may be considered as potential competing interests: